

RESEARCH

Open Access



Ultra-low-defect homoepitaxial micro-LEDs with enhanced efficiency and monochromaticity for high-PPI AR/MR displays

Yibo Liu¹, Guobin Wang³, Feng Feng¹, Mengyuan Zhanghu², Zhengnan Yuan¹, Zichun Li¹, Ke Xu³, Hoi Sing Kwok¹ and Zhaojun Liu^{2*}

*Correspondence:
liuzj@sustech.edu.cn

¹ Department of Electronic and Computer Engineering, The Hong Kong University of Science and Technology, Hong Kong SAR, China

² Department of Electrical and Electronic Engineering, Southern University of Science and Technology, Shenzhen, China

³ Suzhou Institute of Nano-Tech and Nano-Bionics, Chinese Academy of Sciences, Jiangsu Institute of Advanced Semiconductors, Suzhou, China

Abstract

The issue of brightness in strong ambient light conditions is one of the critical obstacles restricting the application of augmented reality (AR) and mixed reality (MR). Gallium nitride (GaN)-based micro-LEDs, renowned for their exceptional brightness and stability, are considered the foremost contenders for AR applications. Nevertheless, conventional heteroepitaxial growth micro-LED devices confront formidable challenges, including substantial wavelength shifts and efficiency droop. In this paper, we firstly demonstrated the high-quality homoepitaxial GaN-on-GaN micro-LEDs micro-display, and thoroughly analyzed the possible benefits for free-standing GaN substrate from the material-level characterization to device optoelectronic properties and micro-display application compared with sapphire substrate. The GaN-on-GaN structure exhibits a superior crystal quality with ultra-low threading dislocation densities (TDDs) of $\sim 10^5 \text{ cm}^{-2}$, which is three orders of magnitude lower than that of GaN-on-Sapphire. Through an in-depth size-dependent optoelectronic analysis of blue/green emission GaN-on-GaN/ Sapphire micro-LEDs from $100 \times 100 \mu\text{m}^2$ shrink to $3 \times 3 \mu\text{m}^2$, real that a lower forward voltage and series resistance, a consistent emission wavelength (1.21 nm for blue and 4.79 nm for green @ 500 A/cm^2), coupled with a notable reduction in efficiency droop ratios (15.6% for blue and 28.5% for green @ 500 A/cm^2) and expanded color gamut (103.57% over Rec. 2020) within GaN-on-GaN $10 \mu\text{m}$ micro-LEDs. Last but not least, the GaN-on-GaN micro-display with 3000 pixels per inch (PPI) showcased enhanced display uniformity and higher luminance in comparison to its GaN-on-Sapphire counterpart, demonstrating significant potentials for high-brightness AR/MR applications under strong ambient light.

Introduction

In recent years, the field of display technology has witnessed remarkable advancements, revolutionizing the way we interact with digital content and enhancing our visual experiences. Among these breakthroughs, micro-LED technology stands out as a promising contender for the next generation of display systems. With its potential to achieve

unprecedented brightness levels, energy efficiency, and pixel density, micro-LED displays hold the key to ushering in a new era of high-resolution, immersive visual displays.

Micro-LED technology represents a significant departure from traditional Liquid Crystal Displays (LCDs) and Organic Light Emitting Diodes (OLEDs). Unlike these conventional technologies, micro-LED displays consist of individual self-emissive micro-sized light-emitting diodes that function as individual pixels. This intrinsic feature allows for superior control over each pixel's brightness and color, thereby leading to sharper images, wider color gamuts, and improved contrast ratios. With the potential to reshape industries like displays [1–5], visible light communication (VLC) [6–8], and medical healthcare applications [9, 10], Micro-LED technology is on the cusp of redefining the limits of technological progress.

The efficiency droop of LEDs has long been a vexing issue in solid-state lighting. When micro-LEDs are applied in display applications, this challenge becomes more pronounced. Taking AR glasses as an example, although micro-LEDs exhibit higher brightness compared to OLEDs and QLEDs at low current densities, their complex optical design and waveguide systems lead to significant light loss during propagation. The Fig. 1(a) illustrates the efficiency issues associated with the use of a diffractive waveguide, which includes the color conversion efficiency of full-color quantum dots,

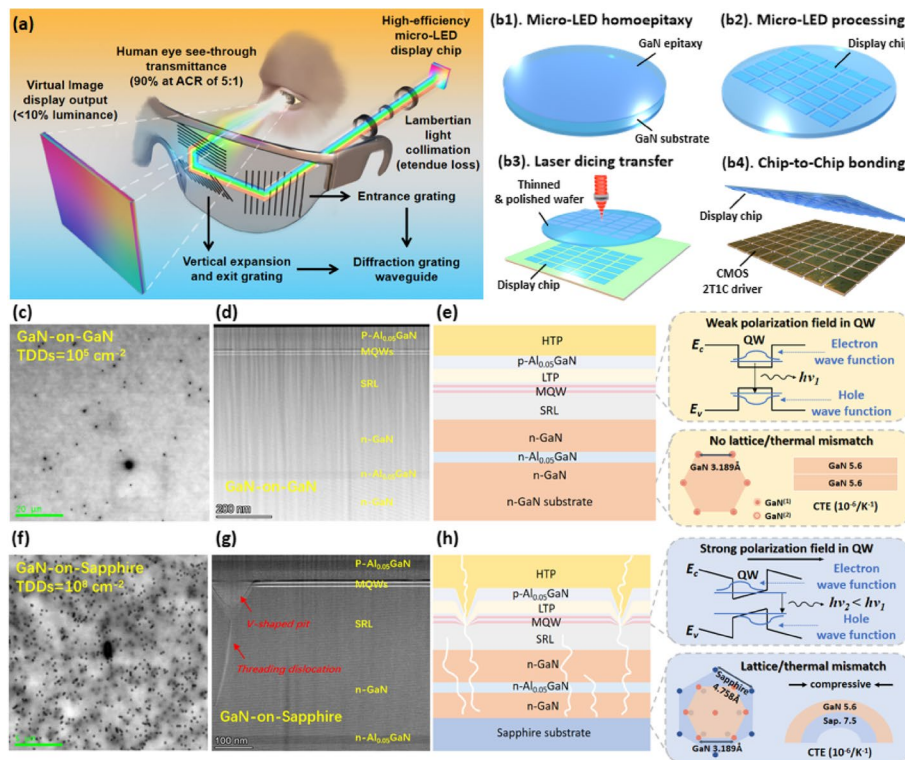


Fig. 1 **a** Efficiency issues in micro-LED AR glass with diffractive waveguide (from Millions of Nits-In and Thousands of Nits-Out); **b** Fabrication process of micro-LED display: 1. micro-LED homoepitaxy; 2. micro-LED processing; 3. laser dicing transfer of thinned and polished homoepitaxy wafer; 4. chip-to-chip bonding mass transfer of micro-LED display chip and CMOS two-transistor one-capacitor (2T1C) driver; **(c), (f)** Cathodoluminescence (CL) characterization, **(d), (g)** Transmission electron microscopy (TEM) observation, **(e), (h)** different polarization field in quantum well (QW) and lattice/thermal mismatch demonstration of GaN-on-GaN homoepitaxy and GaN-on-Sapphire heteroepitaxy structure

collimation efficiency of lens arrays, and the efficiency of light coupling into and out of the waveguide system. Typically, the lens array is designed for collimating micro-LED Lambertian light into semi-collimated light before entering the waveguide system. Then, a small entrance area of waveguide severely limits the coupled light due to “etendue loss” [11]. Under conditions of total internal reflection (TIR), only a fraction of incident light can complete waveguide transmission, resulting in substantial brightness loss. Next, the diffraction grating losses due to the pupil expansion through entrance grating, expansion grating and exit grating. Ultimately, the light that enters through the small entrance area is dispersed throughout the very larger exit area in order to facilitate clear visibility of the image across the whole field of view (FOV). Furthermore, unlike VR glasses, AR glasses are primarily used outdoors where ambient light is stronger. Considering the ambient contrast ratio (ACR), micro-LEDs require higher current drive to achieve the desired brightness for a satisfying user experience. Research [12] indicates that with a waveguide efficiency of 10%, ACR at 5:1, and human eye see-through transmittance of 90%, the luminance at the eye is less than 10% of the luminance at the display output. With the increase in ambient light, the ACR gradually decreases. As shown in Fig. S1, with L_{LED} fixed at 100 k nits, when the optical loss is approximately 1%, L_{on} equals 1 k nits. The $ACR < 5:1$ when $L_{ambient} > 300$ nits (indoors) and $ACR < 2:1$ when $L_{ambient} > 2000$ nits (outdoors). Therefore, enhancing the performance of the display source is one of the solutions to achieve a high ACR. The detailed luminance requirements for various display scenarios are listed in Table S1, the micro-LED needs over 400 A/cm^2 under outdoor sunny condition. Therefore, a lower efficiency droop can ensure that micro-LEDs achieve higher brightness at high current densities, reducing device power consumption and heat generation. Additionally, a stable emission wavelength at different current densities can ensure color accuracy for varying display requirements under changing ambient lighting conditions.

Studies have shown that the causes and explanations for efficiency droop vary widely and can be broadly categorized into three aspects: defect-related mechanisms [13], Auger recombination [14], and electron leakage and overflow [15]. Among these, defect-related mechanisms are more amenable to optimization of efficiency droop by changing substrate materials. Among the many material options for micro-LED substrates, Gallium Nitride (GaN) has emerged as a leading candidate, offering a host of advantages that make it an ideal choice for micro-LED fabrication. Compared to GaN-on-sapphire structure, GaN-on-GaN LED refers to a structure where the epitaxial layers and the active region of the LED are grown on a free-standing GaN (FS-GaN) substrate. This approach offers numerous benefits, such as reduced lattice mismatch, lower threading dislocation densities (TDDs) and improved thermal management [16–19], leading to enhanced device performance, such as shorter peak wavelength shift, lower efficiency droop, higher luminance, better display uniformity. Over the past few decades, numerous researchers have documented that dislocations serve as nonradiative centers within GaN-based LEDs. As a result, the development of epitaxial structures with lower dislocation densities on GaN substrates has garnered significant attention. In a pivotal milestone, back in 1998, Takashi Mukai, Kazunori Takekawa, and Shuji Nakamura [20] reported the first InGaN-based blue LED on a GaN substrate, achieving a dislocation density of $2 \times 10^7 \text{ cm}^{-2}$. Subsequently, in 2007, Akita K et al. [21] achieved an even lower

dislocation density of 10^6 cm^{-2} , accompanied by an enhancement in external quantum efficiency. Moving forward to 2011, two distinct research groups [22, 23] made noteworthy contributions by reporting efficiency droop reduction through the utilization of the GaN-on-GaN structure. However, the dislocation density remains at the level of 10^6 to 10^7 cm^{-2} , accompanied by a noticeable peak wavelength shift.

This work delves into our remarkable progress made in the domain of micro-LEDs on FS-GaN substrate with an ultra-low dislocation density of $\sim 10^5 \text{ cm}^{-2}$ and nearly stress-free state. Figure 1(b) demonstrates the fabrication process of micro-display including micro-LED homoepitaxy, display array processing, laser dicing transfer and chip-to-chip bonding mass transfer, and the detailed information on the fabrication process of the micro-LED display can be referred to the “Materials and methods” section. We have reported the first-ever micro-LEDs display array with a homoepitaxy GaN-on-GaN structure, featuring an ultra-low dislocation density, achieving minimal efficiency droop, consistent emission peak wavelength and an extensive color gamut of 103.57% Rec. 2020. Homoepitaxial blue and green devices manifest a peak shift value (nm) that is merely 10% and 24% of the corresponding value observed in traditional heteroepitaxial structures as the current density increases. Notably, this is concomitant with a substantial 30% enhancement in efficiency. Therefore, our attention will be directed towards a comprehensive exploration of material engineering, device physics, and display applications, and systematically investigate and analyze the exceptional performance exhibited by GaN-on-GaN micro-LED structures.

Results and discussion

Material-level characterization results

To verify the TDD of heteroepitaxial and homoepitaxial structures, the cathodoluminescence (CL) diagrams are characterized shown in Fig. 1(c) and (f). The CL results reveal TDDs of approximately $\sim 10^8 \text{ cm}^{-2}$ and $\sim 10^5 \text{ cm}^{-2}$ for GaN-on-sapphire and GaN-on-GaN, respectively. Furthermore, transmission electron microscopy (TEM) observations in Fig. 1(d) and (g) clearly demonstrate the V-shaped pits with inverted pyramid structure embedded in quantum wells region for GaN-on-Sapphire structure, which usually connect to the threading dislocation and serve as the stress relaxation centers in heteroepitaxy. In contrast, the V-shaped pits can be rarely observed in GaN-on-GaN homoepitaxy due to the lower dislocation density and nearly free-stress structure. Due to the absence of lattice and thermal mismatch between the epitaxial layer and the substrate, the polarization field in homoepitaxial devices is correspondingly reduced, as depicted in Fig. 1(e) and (h). Certain researchers [24–27] posited that V-shaped pits enhance light extraction efficiency (LEE) through promoting reflection and refraction at the boundaries, thereby facilitating the escape of light. And some others [28–30] stated that the lateral diffusion of excited carriers into non-radiative recombination centers at TDs could be effectively suppressed by the presence of V-pits, thereby improving the quantum efficiency. However, previous findings [31–33] indicated the center of V-pits connected to dislocations are known as non-radiative recombination region and may increase the leakage current as well, which may degrade the quantum efficiency. Therefore, the ultimate change in external quantum efficiency (EQE) depends on various factors such as the density, structure,

and size of the V-shaped pits [30, 34]. It remains an open question and the discussion regarding V-shaped pits will continue in the subsequent EQE analysis section of this paper.

The X-ray diffraction (XRD) rocking curves for (002) and (102) scans are presented in Fig. 2(a) and (b). The symmetric (002) and asymmetric (102) rocking curves full width at half maximum (FWHM) represent the influence of screw dislocation density and edge dislocation density, respectively [35]. The FWHM values of the (002) scan are approximately 257.7 arcsec and 44.4 arcsec for GaN-on-sapphire and GaN-on-GaN structures, respectively. For the (102) scan, the FWHM values are 321.9 arcsec and 32.8 arcsec for GaN-on-sapphire and GaN-on-GaN structures, respectively. The GaN-on-sapphire structure exhibits noticeable broadening in both symmetric and asymmetric rocking curves. The FWHM from rocking curve can be used to estimate screw and edge dislocation densities. Typically, the sum of these two values represents the threading dislocation densities (TDDs) [36], with the Eq. (1) as follows:

$$\rho_{(s,e)} = \frac{W_{(s,e)}^2}{2\pi \ln 2 \cdot b_{(s,e)}^2} \quad (1)$$

where s represents the screw dislocation (002 scan) and e represents the edge dislocation (102 scan). ρ represents the dislocation densities calculated. W is the FWHM value, and b denotes the Burgers vector, which should be equal to the lattice parameters ($b_s = c(\text{GaN}) = 0.52$ nm and $b_e = a(\text{GaN}) = 0.32$ nm). Through the calculation, the TDD for GaN-on-GaN and GaN-on-Sapphire structures are determined to be 7.09×10^5 cm⁻² and 4.34×10^8 cm⁻² respectively, indicating lower TDDs and better crystal quality for GaN-on-GaN structure, which is consistent to CL results.

In order to characterize the strain states of the GaN-on-GaN and GaN-on-Sapphire structures, micro-Raman scattering spectroscopy was employed in conjunction with a 25 mW He-Ne laser operating at 632.8 nm. The E_2 phonon peak, which is determined to be 567.36 cm⁻¹ for a stress-free GaN thin film, is sensitive to the stress of the epitaxial structure [37]. The phonon peak at E_2 for GaN-on-Sapphire is 567.52 cm⁻¹, while it is 570.29 cm⁻¹ for GaN-on-GaN, as illustrated in Fig. 2(c). Using Eq. (2), the relaxation of residual stress can be calculated.

$$\sigma = \Delta\omega/k(\text{cm}^{-1}\text{GPa}^{-1}) \quad (2)$$

where $\Delta\omega$ denotes the E_2 phonon peak shift, σ represents the biaxial stress, and k stands for the GaN E_2 mode Raman strain coefficient (4.2 cm⁻¹/GPa). The calculation reveals that the GaN-on-GaN structure is in close proximity to an ideal stress-free state (~ 0.010 GPa), whereas the GaN-on-Sapphire structure has a compressive stress of ~ 0.698 GPa. This value suggests that the inherent strain within the homoepitaxy structure has been alleviated, resulting in a diminished Quantum-confined Stark Effect (QCSE). Consequently, there are more overlaps between electron-hole wave functions and increased radiative recombination. To further prove this point, the room-temperature time-resolved photoluminescence (TRPL) was performed at the peak emission of MQWs by using the FS5 Spectrofluorometer integrated with Life Spectrometer, manufactured by Edinburgh Instruments Ltd. It is based on the Time Correlated Single Photon Counting

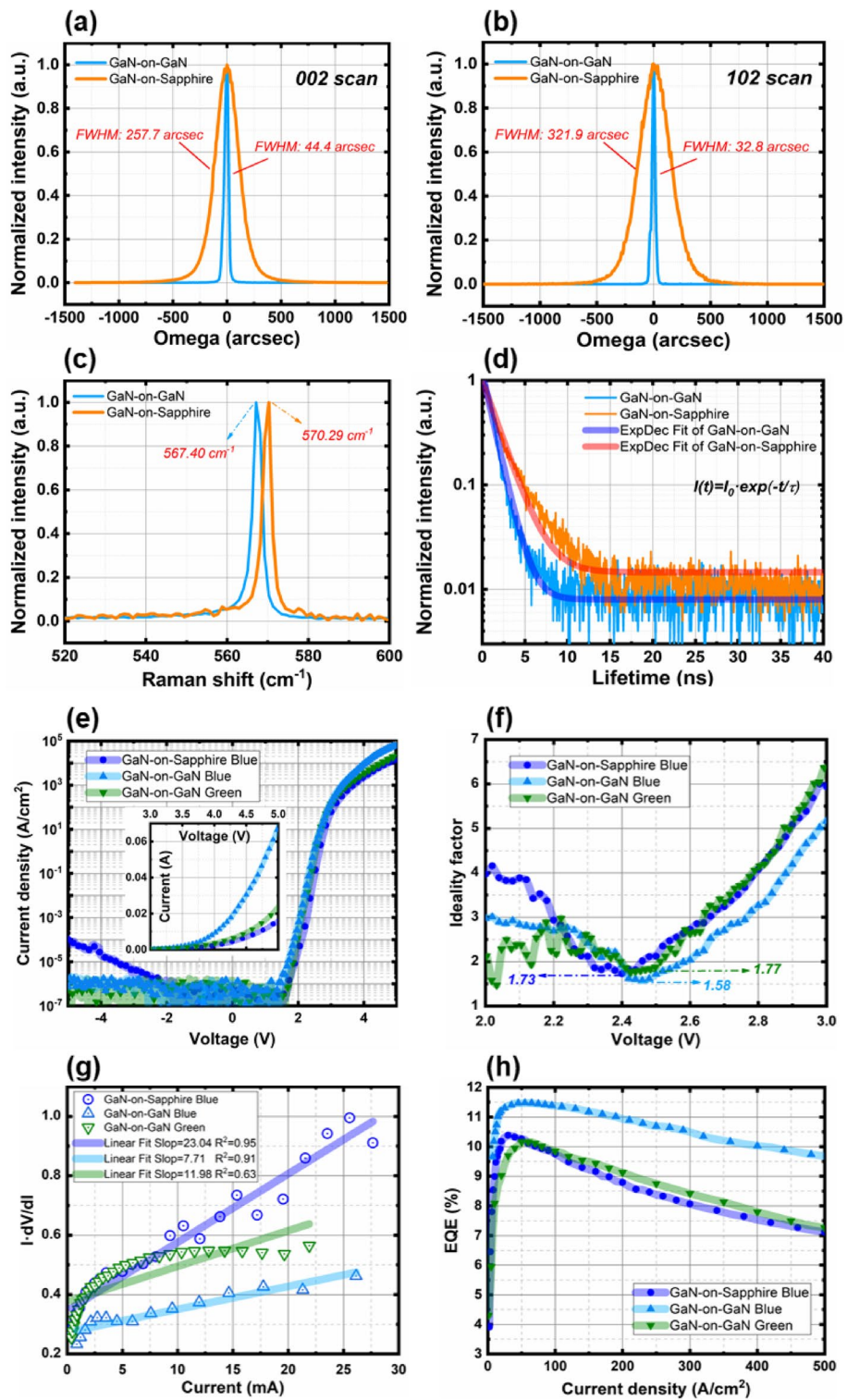


Fig. 2 **a** Symmetric and **(b)** Asymmetric rocking curves; **c**: micro-Raman scattering spectra; **d** room-temperature time-resolved photoluminescence (TRPL) decay of GaN-on-Sapphire and GaN-on-GaN structure respectively; **e** current–voltage (I-V) and current density–voltage (J-V) characteristics; **f** ideality factor extraction within 2–3 V; **g** series resistance extraction; **h** EQE characteristics of three types of micro-LED

(TCSPC) technique, including the Xe Arc nanosecond flash lamp with 325 nm wavelength emission, TCSPC data acquisition card and photomultiplier tube detector. The carrier lifetime was extracted via a single exponential decay model, which is 1.19 and 1.82 ns for GaN-on-GaN and GaN-on-Sapphire respectively, as illustrated in Fig. 2(d). In GaN/InGaN micro-LEDs, On one hand, a high density of defects can facilitate the trapping of carriers during transport, consequently leading to a reduction in their lifetime. On the other hand, the separation of electron and hole wavefunctions induced by the QCSE diminishes the probability of recombination, thereby prolonging the lifetime. In our case, after confirming the lower defect density in the GaN-on-GaN structure through CL and XRD measurements, we attribute the observed shorter lifetime of GaN-on-GaN to a weakening of the QCSE phenomenon, better material qualities, lower defect density and more electron–hole wave function overlaps [38], which also suggests the faster response time and higher modulation bandwidth for GaN-on-GaN structure micro-LEDs VLC. In addition, the Transmission Line Model (TLM) was employed to examine the ohmic contacts between p-GaN and CSL(ITO) layer within distinct substrate structures, as shown in Fig. S3. The results reveal that the contact resistance of the GaN-on-GaN structure ($R_{contact} = 958.2 \Omega$) and the sheet resistance ($R_{sheet} = 2.73 \times 10^4 \Omega/\square$) are both lower than those of the GaN-on-Sapphire structure ($R_{contact} = 1751.0 \Omega$ and $R_{sheet} = 5.31 \times 10^4 \Omega/\square$). Also, the specific contact resistivity ($\rho_{contact}$) between ITO and p-GaN layer can be calculated as $3.35 \times 10^{-3} \Omega \cdot \text{cm}^2$ for GaN-on-GaN and $5.78 \times 10^{-3} \Omega \cdot \text{cm}^2$ for GaN-on-Sapphire respectively. A comparison of AFM images shown in Fig. S4 reveals that the GaN-on-GaN surface is more uniform and well-defined compared to GaN-on-Sapphire. Additionally, clear crystallographic steps can be observed, indicating better crystalline quality and a smoother surface for p-GaN in the homoepitaxial structure, contributing to achieving lower sheet resistance and contact resistance.

Device-level analysis and discussion

In this section, characterization is conducted on three types of samples: GaN-on-Sapphire blue, GaN-on-GaN blue, and green with size from $100 \times 100 \mu\text{m}^2$ shrinks to $3 \times 3 \mu\text{m}^2$. The epi-ready wafer sizes are 2-inch for GaN-on-Sapphire blue and GaN-on-GaN blue, and $10 \times 10 \text{ mm}^2$ for GaN-on-GaN green. The DC-voltage characteristics were measured by using Keysight B1500 Analyzer. The size-dependent current–voltage (I - V) related characterizations including current density–voltage (J - V) and ideality factor extraction for all three are individually demonstrated in Fig. S5, and the relevant analysis can refer to the following content of Fig. S5 in Supplementary Information. Figure 2(e) illustrates the I - V in linear scale and J - V in semi-log scale behaviors for $10 \times 10 \mu\text{m}^2$ micro-LEDs. If we define a current density of $1 \text{ mA}/\text{cm}^2$ as the threshold for LED activation, the turn-on voltage for GaN-on-Sapphire blue devices is 2.26 V. For GaN-on-GaN devices in blue, and green, the respective turn-on voltages are 2.05 V and 2.09 V. Among them, the GaN-on-GaN blue micro-LEDs exhibit significantly lower turn-on voltages and markedly superior current density capabilities compared to the other two. The current density is measured as 15,810, 68,240 and $23,790 \text{ A}/\text{cm}^2$ at a driving voltage of 5 V for GaN-on-Sapphire, GaN-on-GaN blue and green respectively. In contrast to the higher indium composition in GaN-on-GaN green devices, the lower indium composition in the active region of GaN-on-GaN blue micro-LEDs can mitigate internal

piezoelectric polarization, thereby improving radiative recombination efficiency of carriers in small-sized devices. Additionally, compared to GaN-on-sapphire blue devices with elevated dislocation density, the lower dislocation density in GaN-on-GaN devices signifies a more complete lattice structure, facilitating reduced hindrance to carrier diffusion and transportation processes within the device. The resultant reduction in localized carrier recombination due to dislocations contributes to sustaining higher current densities. The reverse leakage current density is $\sim 10^{-4}$ and $\sim 10^{-7}$ A/cm² level at -5 V for GaN-on-Sapphire and GaN-on-GaN micro-LEDs respectively, which can be attributed to the increased leakage path in higher dislocation densities GaN-on-Sapphire structure. The evident carrier leakage also contributes to a lower current injection efficiency and an increase in defect-induced recombination within the GaN-on-Sapphire micro-LEDs.

The value of the ideality factor (n) is a parameter that indicates the mechanism of current transport within the device, and the derivation process can be found in Supplementary Information. As the Shockley theory applied to traditional p-n junction diodes, when n approaches 1, it corresponds to band-to-band radiative recombination, which is associated with diffusion current. Conversely, when n approaches 2, it is linked to Shockley-Read-Hall (SRH) recombination involving traps, which contributes to recombination current. However, our previous research [39] indicated the higher ideality factor in GaN-based MQWs LED primarily stem from the diode superposition within the LED structure. In addition to the GaN p-n junction, the quantum barriers heterojunction within the quantum well region also needs to be considered. This is a significant factor leading to the difference in ideal factors between homoepitaxy blue and green micro-LEDs. The process of calculating the ideality factor through the I - V curve can be referenced to the Eq. (S2) [40]. As the driving voltage increases, the ideality factor n exhibits a minimum value, representing the device's state closest to ideal performance shown in Fig. 2(f). This minimum value typically occurs after LED turn-on, during the initial stages of low current density injection. Ideality factor values greater than 2 in this context result from intrinsic parallel resistances and nonradiative recombination caused by deep-level defects in quantum wells, which dominate the current transport mechanism. The lowest value of ideality factor is 1.74, 1.58, and 1.77 for GaN-on-Sapphire blue, GaN-on-GaN blue and green respectively. With the rise in injection current, the series resistance prompts a decline in voltage, resulting in a growing disparity between the real and theoretical currents. This divergence leads to a curvature in the current-voltage graph, ultimately inducing a rise. Within the operating range of 2.5-3 V, the variation in the ideal factor values for all three corresponds to the sequence of their respective minimum values, indicating that GaN-on-GaN blue micro-LED operates in the most ideal state. The high defect density in GaN-on-Sapphire blue micro-LED significantly increases the non-uniformity of the quantum barrier, leading to tunneling mechanism and an increase in the ideal factor [40]. In the case of GaN-on-GaN green micro-LED, the increase in indium composition in the MQWs results in a more pronounced rectification characteristic in the heterojunction, leading to the highest ideal factor, which indicates that junction superposition predominates in the analysis above.

Figure 2(g) demonstrate $I \cdot dV/dI$ vs. I relation to extract the series resistance (R_s) of three kinds of micro-LEDs with size of $10 \times 10 \mu\text{m}^2$, and the data for other sizes can be found in Fig. S6-S8. It is worth noting that the linear fit of R_s calculation for GaN-on-GaN

green devices is notably poorer-fitted compared to other devices, particularly evident in the R-square value of 0.63. Consequently, the precision of R_s values calculation for green devices less than 10 μm is diminished in comparison to other devices, suggesting that the high indium composition in the MQWs region of the green LED induces instability in the interface states between the EBL and the barrier region of MQWs due to polarization effects, exacerbating carrier leakage at low current densities and carrier overflow under high current density injection [41, 42]. The R_s values for GaN-on-Sapphire and GaN-on-GaN blue micro-LEDs are 23.04 and 5.78 Ω , respectively. Since R_s primarily originates from the high-resistance p-GaN region, a reasonable explanation would be that the doping efficiency of Mg was boosted in the homoepitaxy structure [43]. In reference to the analysis of size dependence concerning R_s and n , please refer to Fig. S9 as detailed.

As for the EQE measurement, the light output power was measured by XPQY-EQE-Adv Integrating Sphere and the EQE was calculated through Eq. (3) and (4):

$$EQE = \frac{P/h\nu}{I/e} \quad (3)$$

$$EQE = LEE \times IQE = LEE \times \frac{CIE \times Bn^2}{An + Bn^2 + Cn^3} \quad (4)$$

$$n = \frac{J \times \tau}{e \times d} \quad (5)$$

where P represents the light output power, h stands for the Planck constant, and ν is derived from c/λ , wherein c signifies the speed of light, and λ represents the emission peak wavelength achieved with a specific current density injection. I and e represent the injected current and the elementary charge of an electron respectively. In essence, the numerator in Eq. (3) corresponds to the number of emitted photons, while the denominator segment represents the number of injected electrons. In Eq. (4), LEE signifies the light extraction efficiency, while IQE denotes the internal quantum efficiency. The IQE can be expounded using the ABC model, where CIE represents the current injection efficiency, indicating the proportion of effective carriers in the active region. n stands for carrier concentration, while A , B , and C represent the coefficients for Shockley–Read–Hall (SRH), radiative, and Auger recombination, respectively. Equation (5) [44] facilitates the conversion between carrier concentration (n) and current density (J), where τ represents carrier lifetime shown in Fig. 2(d), and d stands for the active region thickness.

The brightness of micro-LEDs is closely associated with their EQE. A lower degradation in EQE ensures that the devices maintain a higher level of brightness even when operating at high current densities. Refer to Fig. S10(a) and (b) for the radiometric unit of light output power (W) and photometric unit of luminous flux (lm) results measured from integrating sphere. The measurement indicates that the light output power of GaN-on-GaN blue devices is significantly superior to other devices, reaching 0.13 mW at 500 A/cm^2 . GaN-on-GaN green and GaN-on-sapphire blue devices maintain a lower level, achieving 0.09 and 0.08 mW at 500 A/cm^2 respectively. Furthermore, GaN-on-GaN green exhibits the highest luminous flux, which can be attributed to the human

eye's visual response being more sensitive to green light. Under the same optical power, green LEDs have higher luminous flux and luminous efficacy, but they also demonstrate a more pronounced phenomenon of luminous efficacy droop. GaN-on-GaN green can achieve a luminous flux of 15.0 mlm at 500 A/cm², followed by GaN-on-GaN blue at 7.3 mlm, and GaN-on-Sapphire blue with the lowest at 3.8 mlm. Based on that, we could infer that panel brightness for micro-display is directly correlated with luminous flux, and the brightness of GaN-on-GaN green is more than twice that of blue. Figure 2(h) displays the EQE performance for three types of micro-LEDs. The peak EQE values are 10.39% for GaN-on-Sapphire blue, 11.48% for GaN-on-GaN blue, and 10.16% for GaN-on-GaN green micro-LEDs respectively, and the EQE droop ratios are 31.3%, 15.6% and 28.5%. The ratio is defined as the value difference between the device peak EQE and the EQE at a current density of 500 A/cm², divided by the peak EQE value. Regarding peak EQE, it is intricately linked to IQE and LEE, and a more detailed discussion on this matter will be provided in the following sections. The current density at the peak EQE (J_{peak}) is another noteworthy aspect shown in Fig. S10(d), where a distinct observation emerges—the J_{peak} of GaN-on-GaN micro-LEDs stands notably higher than that of GaN-on-Sapphire counterparts. Guided by the derivation of the ABC model, J_{peak} demonstrates a direct proportionality to $\sqrt{A/C}$. Based on the previous analysis, we ascertain that the A parameter, linked to GaN-on-GaN devices and lattice defects, is smaller compared to GaN-on-Sapphire devices. As a result, we attribute the elevated J_{peak} to a smaller C parameter, which in turn correlates to Auger recombination. As mentioned above that Auger recombination is one of the contributor to EQE droop. Thus, the diminished value of parameter C concurs with the aforementioned analysis, suggesting a low EQE degradation in GaN-on-GaN devices.

For further investigation, the Fig. 3(a)-(c), involving a more detailed ABC model fitting and parameters extraction with various sizes, will further substantiate this viewpoint. The scattered points in the Fig. 3(a)-(c) represent the IQE data, employing the room-temperature reference-point method (RTRM) [45] to deduce IQE data from EQE measurements. The solid line represents model fitting based on Eq. (3). Detailed results of the EQE tests can be referred to in Fig. S10(e)-(g), and the specific values of each parameter can be referred to Table S2-S4. Micro-LEDs of three kinds with a size of 100 μm achieve an IQE above 90%, a relatively high level. However, as the size decreases, the IQE progressively reduces. This reduction is attributed to an increase in the defect-assisted recombination coefficient (A) for smaller-sized devices and a decrease in CIE, as illustrated in the Fig. 3(e) and (f). These factors collectively reflect an increase in non-radiative recombination due to defects and surface recombination, as well as carrier leakage. With decreasing size, an increasing trend in the A coefficient is observed for all three types of devices. The trend is most pronounced for GaN-on-Sapphire due to its high intrinsic defect density. Concurrently, the CIE for GaN-on-Sapphire blue, GaN-on-GaN blue, and green decreases from 93%, 99%, and 98% at 100 μm to 50%, 73%, and 62% at 5 μm , respectively. This implies that sidewall surface recombination and internal defects causing carrier leakage and overflow are most severe in GaN-on-Sapphire blue, followed by GaN-on-GaN green, and with the least impact on GaN-on-GaN blue. Moreover, as illustrated in Fig. 3(d), the LEE of all three devices exhibits an upward trend as their dimensions diminish. The observed rise can be ascribed to the increased percentage of

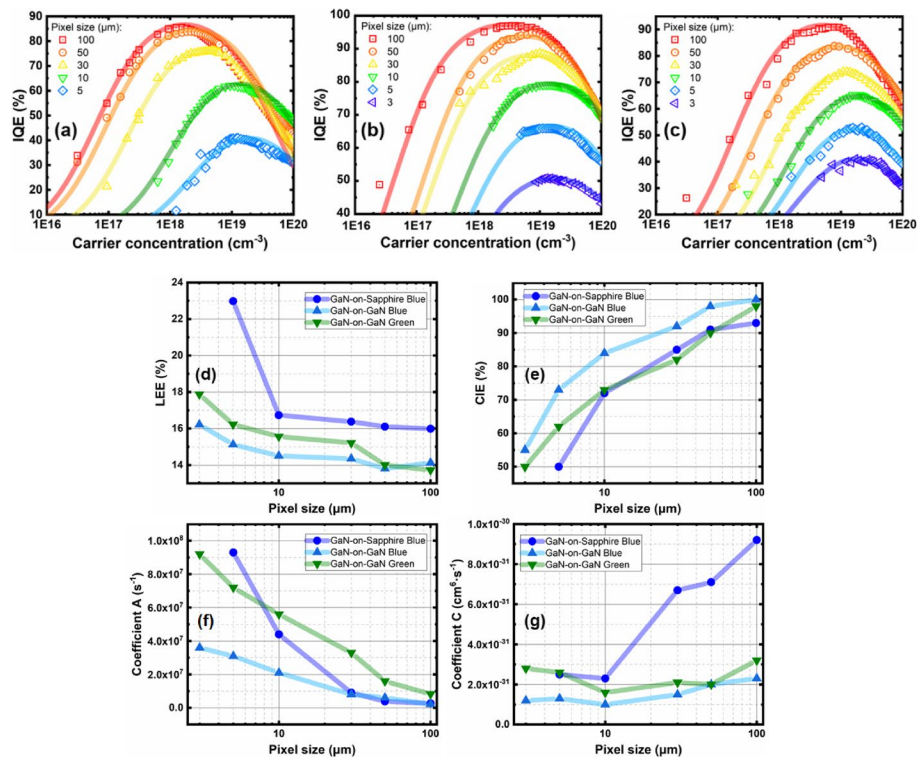


Fig. 3 Size-dependent internal quantum efficiency (IQE) of (a) GaN-on-Sapphire blue, (b) GaN-on-GaN blue and (c) GaN-on-GaN green micro-LEDs with ABC model fitting; **d** light extraction efficiency (LEE), **e** current injection efficiency (CIE), **f** coefficient A and **g** coefficient C with different pixel size

edge-emitting light in small-sized devices. Combined with a shorter overall light path, which leads to a reduction in losses caused by internal refraction, reflection, and scattering within the device. The substantial V-pit density accounts for the elevated LEE of sapphire substrates, which will be discussed in subsequent sections. The LEE trends for blue and green devices on GaN substrates show no significant difference, with green being only up to 2% higher than blue. This minor discrepancy is attributed to the variation in the refractive index of GaN-based materials for different wavelengths of light. Figure 3(g) illustrates the variation of the Auger recombination coefficient (C) with size, where C is commonly considered to be a multi-carrier process associated with the generation of thermal energy [46]. In comparison to GaN-on-Sapphire blue micro-LEDs, GaN-on-GaN blue and green micro-LEDs exhibit no significant size dependency. This can be attributed to the exceptional thermal dissipation properties of the GaN substrate. The superior thermal management offered by the GaN substrate reduces the thermal effects related to Auger recombination, thereby maintaining a consistent Auger recombination coefficient irrespective of the size variations.

Next, we primarily focus on the spectral characterization of GaN-on-GaN blue and green micro-LEDs. Figure 4(a) illustrates their intensity-normalized electroluminescence (EL) spectra. The emission center wavelengths for the blue and green micro-LEDs at 10 A/cm^2 are 455.6 nm and 504.3 nm respectively. The corresponding FWHM values are 18.6 nm and 23.5 nm. The varying FWHM of the EL peaks, corresponding to

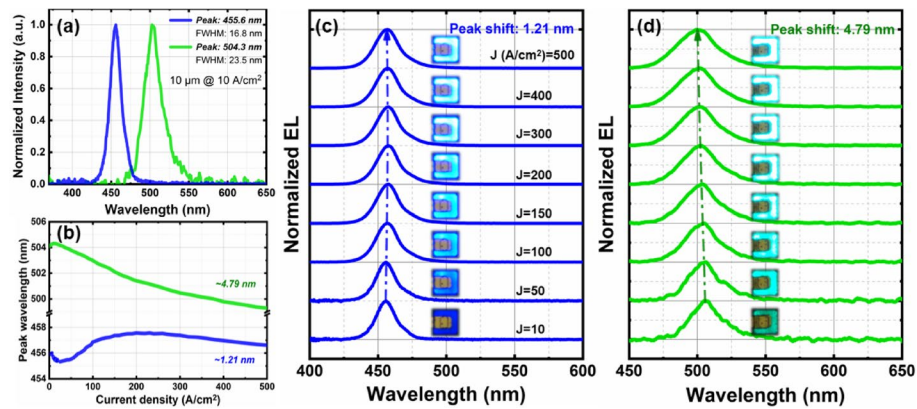


Fig. 4 **a** Normalized EL of GaN-on-GaN blue and green micro-LEDs @ 10 A/cm²; **b** Peak wavelength shift with current density elevating to 500 A/cm²; Specific EL spectra from 10 to 500 A/cm² with luminous images of GaN-on-GaN **(c)** blue and **(d)** green micro-LED

the emission wavelengths, can be attributed to distinct fluctuations in indium composition within the InGaN active layer [47]. The value of FWHM tends to broaden with the increase in current density (data for blue micro-LED will be revealed in the subsequent section; refer to Supplementary Information Fig. S11 for green micro-LED). This indicates that the GaN-on-GaN blue micro-LEDs belong to the typical blue light spectral range, and the green micro-LED is positioned in the spectral range close to cyan.

The peak wavelength shift diagram for both is shown in Fig. 4(b) and the specific shifting with spectra and luminous images from 10 to 500 A/cm² are demonstrated in Fig. 4(c) and (d). It can be observed that the wavelength shift is most pronounced in the case of green light (4.79 nm), followed by blue light (1.21 nm), which originates from varying degrees of the QCSE caused by indium fluctuation within the active region [48, 49]. The polar MQWs possess a built-in electric field that induces band tilting. As the carrier density rises, this leads to a partial screening of the initial built-in field, causing a decrease in the emission wavelength equivalent to a leftward shift in the spectrum, and this shifting is more pronounced with higher In-content in MQWs. More importantly, our GaN-on-GaN devices exhibit the ability to maintain a more stable center wavelength compared to other substrates, benefiting from the fact that lower defect density typically helps mitigate the extent of wavelength blue shift.

Moving forward, we will conduct a comprehensive analysis to contrast the disparities between GaN-on-GaN and GaN-on-Sapphire 10 μm blue micro-LEDs concerning their optical and electrical characteristics. Figure 5(a) showcases the distinction in IQE between the two devices. From the fitting results, the GaN-on-GaN device's A, B, and C parameters are $2.1 \times 10^7 \text{ s}^{-1}$, $5 \times 10^{-11} \text{ cm}^3 \text{ s}^{-1}$, and $1 \times 10^{-31} \text{ cm}^6 \text{ s}^{-1}$, respectively, whereas the GaN-on-Sapphire device's A, B, and C parameters are $4.4 \times 10^7 \text{ s}^{-1}$, $4.3 \times 10^{-11} \text{ cm}^3 \text{ s}^{-1}$, and $2.3 \times 10^{-31} \text{ cm}^6 \text{ s}^{-1}$, respectively. Additionally, the GaN-on-Sapphire device demonstrates a current injection efficiency of 72.2% in contrast to the GaN-on-GaN device of 84.0%. Meanwhile, its LEE reaches 16.7%, outperforming the GaN-on-GaN device's 14.5%. From our results, the more defects connected to V-pits may play a role in enhancing non-radiative and Auger recombination for GaN-on-Sapphire device. This contributes to a elevated leakage current, reduced current injection

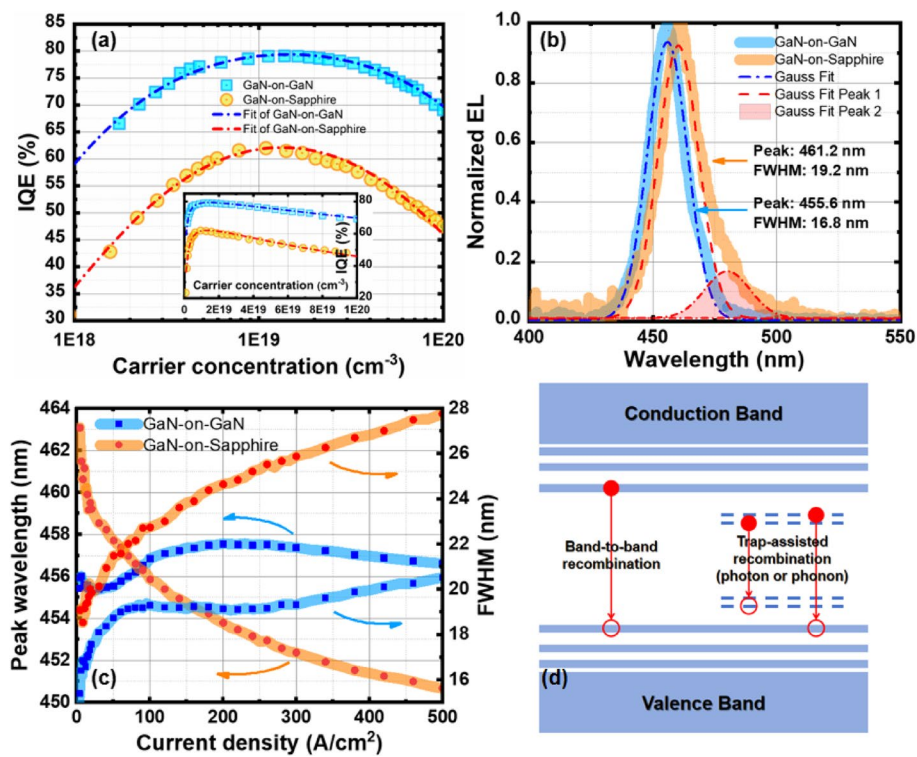


Fig. 5 GaN-on-GaN and GaN-on-Sapphire blue micro-LED: **a** IQE extraction based on room-temperature reference-point (RTRM) method; **b** Peak wavelength shift and FWHM broadening; **c** Intensity-normalized EL with sub-peak fitting; **d** band diagram of trap-assisted recombination

efficiency and a more pronounced droop. Conversely, the V-pits' inverted pyramid structure in active region elevates the device's light extraction efficiency.

To further compare the EL characteristics, the peak wavelength shift and FWHM broadening are demonstrated in Fig. 5(b), the GaN-on-Sapphire micro-LED displays a continuous wavelength shift, ranging from 463 to 451 nm, whereas the wavelength shift for the GaN-on-GaN micro-LED is merely 1.21 nm. One possible explanation might be the reduced compressive stress in homoepitaxial structure and alleviated inherent strain within epilayer, leading to a diminished QCSE in MQWs region [50]. Notably, the wavelength shift of the GaN-on-GaN device can be divided into three intervals. The first interval, 0–20 A/cm², experiences a blue shift due to the band filling effect at low current densities [51–53]. Within the range of 50–200 A/cm², a red shift phenomenon emerges, indicating the gradual influence of device self-heating and the screening effect of external electric fields. The red shift signifies the dominance of the self-heating effect. The third interval (>200 A/cm²) blue shift indicates the dominance of electric field screening due to the QCSE aforementioned. For the GaN-on-Sapphire device, due to the initial pronounced QCSE polarization phenomenon, the electric field shielding effect dominates after the band filling effect, leading to a continuous wavelength blue shift. Similarly, concerning the changes in FWHM, both device types initially experience a rapid increase in FWHM during the band filling effect interval. However, in the subsequent interval, the increase in FWHM for the GaN-on-GaN device is significantly smaller than that for the GaN-on-Sapphire device.

For display application, GaN-on-GaN micro-LEDs offer a narrower FWHM, signifying elevated color purity and an expanded color gamut. This attribute has the potential to significantly heighten the final display performance. Our specific analysis is conducted through fitting the EL spectra. Figure 5(c) shows the EL spectra on two distinct substrates at 10 A/cm². The blue dash-dot line corresponds to the Gaussian fit of the GaN-on-GaN device spectrum, demonstrating an almost ideal fit (R-square = 0.99). The red dash-dot line represents the Gaussian fit of the GaN-on-Sapphire device spectrum. Given the less-than-ideal single-peak fit, a dual-peak Gaussian fit was employed. Notably, a sub-peak emerges at a lower energy position. This sub-peak can be attributed to trap-assisted recombination arising from a higher defect density, as depicted in Fig. 5(d). This recombination mechanism can emit photons or phonons, with photon energy lower than that of band-to-band recombination. It is important to highlight that with the increase in carrier density, the prominence of trap-assisted recombination grows, contributing to the progressively widening divergence in FWHM between the two devices.

The spectral characteristics of micro-LEDs have a direct impact on the color gamut within the color space. The role of a high gamut paired with elevated color purity is pivotal in achieving a display with rich and vibrant colors. We conducted a spectral analysis of the aforementioned 10 μm devices across varying current densities, translating the results into the International Commission on Illumination (CIE) 1976 uniform chromaticity space (UCS). This choice was made due to its suitability for observing shifts in blue spectrum. From the data presented in Fig. 6(a), it becomes evident that GaN-on-GaN blue and green micro-LEDs can attain 103.57% of the Rec. 2020 color gamut at a current density of 10 A/cm². As the current density is ramped up to 500 A/cm² (the direction of the arrow represents an increase in current density), the green emission from the GaN-on-GaN device exhibits noticeable drift, whereas the stability of the blue emission allows it to maintain 92.82% of the Rec. 2020 standard. In Fig. 6(b) and (c), we offer a detailed color coordinates for the three device types. To establish a visually consistent color space for consistent brightness levels, the CIE 1976 color space employs color coordinates u' and v' to quantify color differences [54, 55]. Notably, the human eye's discernible color difference threshold is recognized as 0.005 within the CIE 1976 color space ($\Delta u'v'$) [56, 57].

From Fig. 6(d) and (e), a clear pattern emerges: both GaN-on-Sapphire blue and GaN-on-GaN green devices exhibit a linear increase in color difference values with the progressive increment of current density. For reference, we establish the color coordinates at 10 A/cm² as the baseline, representing a color difference of 0 at this particular current density. Upon reaching a current density of 500 A/cm², the color difference for GaN-on-Sapphire blue measures 0.00145, while for GaN-on-GaN green, it is 0.00066—both values well below the discernible threshold of the human eye (0.005). What's particularly interesting is that the color difference of GaN-on-GaN blue micro-LED does not showcase a distinctly linear correlation with current density. The maximum color difference occurs at a current density of 200 A/cm², registering a mere 2×10^{-5} . This outcome can be attributed to its consistent peak wavelength and narrower FWHM.

To enhance the comparative analysis of our devices' performance, we selected representative blue and green micro-LEDs from peer institutions. Subsequently,

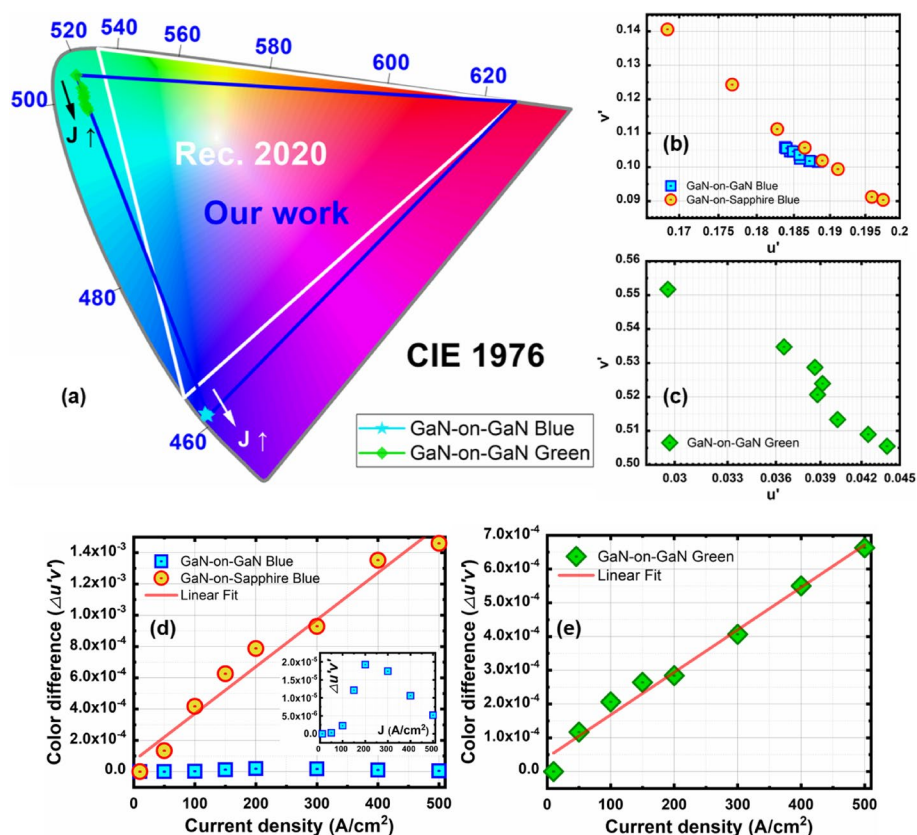


Fig. 6 a Color coordinates of our GaN-on-Sapphire blue, GaN-on-GaN blue and green micro-LEDs in CIE 1976 color space compared with Rec. 2020; b and c) Specific color coordinates (u', v'); d and e) Color difference ($\Delta u'v'$) of GaN-on-GaN/GaN-on-Sapphire blue and GaN-on-GaN green micro-LEDs respectively

comprehensive benchmarking was constructed in Table 1, encompassing both the realms of electrical and optical attributes.

Display-level demonstration

Due to the limitations in the size of the GaN-on-GaN epi-ready wafer for green light, the subsequent device-level processes are exclusively focused on blue micro-LEDs. In the perspective of array displays, we employed a silicon-based driving CMOS two-transistor one-capacitor (2T1C) architecture, which is designed by Shenzhen Sitan Technology CO., Ltd, and conducted a comparative analysis between GaN-on-Sapphire and GaN-on-GaN blue micro-LEDs under full-screen illumination conditions (depicted in Fig. 7(a) and (b)). The devices exhibited a pixel per inch (PPI) of 3000, a resolution of 1300×720 , and a display dimension of $6.5 \times 10.9 \text{ mm}^2$ (refer to the scale diagram of a prototype in Fig. S12). Notably, the GaN-on-GaN devices demonstrated superior brightness and luminosity uniformity in comparison to their GaN-on-Sapphire counterparts. SEM array images (depicted in Fig. 7(c)-(f)) exhibit identical device sizes as those shown in Fig. 7(a) and (b). Due to the implementation of our optimized dual-layer passivation approach, there is no noticeable indium infiltration observed in both the Mesa and n-GaN regions beneath the p- and n-contact indium bumps shown in Fig. 7(d) and (f).

Table 1 Benchmarking of micro-LEDs performance

	Blue micro-LED					Green micro-LED				
	Our work	Our work	Nanjing Univ. * MERGEFORMAT [58]	NTHU * MERGEFORMAT [59]	UCSB * MERGEFORMAT [60]	Our work	Our former work * MERGEFORMAT [61]	KAUST * MERGEFORMAT [62]	Fudan Univ. * MERGEFORMAT [63]	Hanyang Univ. * MERGEFORMAT [64]
Substrate	GaN	Sapphire	PSS	PSS	Sapphire	GaN	PSS	Sapphire	Silicon	Sapphire
Pixel area (μm^2)	100 x 100 to 3 x 3	100 x 100 to 3 x 3	25 π	8 x 8	25 π	100 x 100 to 3 x 3	10 x 10	20 x 20 array	100 π	50 x 50
Forward Voltage (V_f) (V@A/cm ²)	2.66/2.71 @10/20	2.80/2.86 @10/20	2.90 @10	2.73 @22.2	~2.67 @10	2.64/2.72 @10/20	2.36/2.44 @10/20	~2.63/2.87 @10/20	2.5 @1	~2.77 @10
Series resistance (R_s) (Ω)	5.78	23.04	-	3418	-	11.98	34.48	-	-	-
Ideality factor	1.59	1.74	-	1.87	>2	1.77	1.38	-	-	~2
Reverse current (pA@V)	~0.5 @-5	~100 @-5	-	~0.1 @-5	~30 @-10	~0.5 @-5	~1 @-5	~4 x 10 ⁷ @-5	~4 x 10 ⁵ @-5	~50 @-5
Peak wavelength (nm)	455.6	460	465	452.5	455	504.3	518	-	517.5	~525
Peak shift (nm@A/cm ²)	1.21 @500	9.4 @500	5 @20	~9 @500	15 @1000	4.79 @500	10.5 @500	-	~20 @500	9.06 @1.4
FWHM (nm@A/cm ²)	16.8 @10	18.9 @10	17 @1	15.7 @17	-	23.5 @10	29.2 @10	-	~29 @10	~30 @1
FWHM Broadening (nm@A/cm ²)	3.73 @500	8.9 @500	3.5 @10	~3.7 @500	-	8.36 @500	10.54 @500	-	~9 @500	-
Peak EQE	11.52%	10.39%	11.47%	13.86%	~9%	10.16%	16%	2.67%	~2%	-
EQE droop ratio (@A/cm ²)	15.6% @500	31.3% @500	39.8% @100	~30% @500	~40% @500	28.5% @500	62.5% @500	-	~60% @500	47% @100

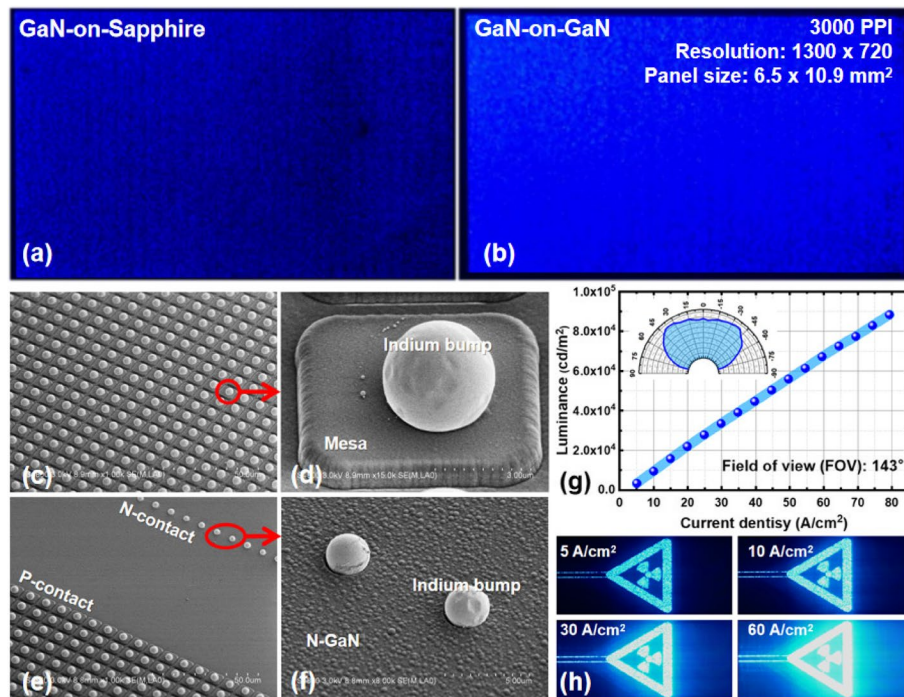


Fig. 7 **a, b** Display uniformity of GaN-on-Sapphire and GaN-on-GaN micro-LED array; **c-f** scanning electron microscope (SEM) observation of reflowed indium bumps onto Mesa structure and n-GaN layer; **g** Luminance vs. driving current density relationship with the light distribution curve inset; **h** Display pattern luminance graph from 5 to 60 A/cm²

Considering the superior performance exhibited by GaN-on-GaN blue micro-LEDs, which is selected for the subsequent packaging and integration processes with peripheral drivers. The panel luminance and field of view (FOV) for GaN-on-GaN blue micro-LED display is measured as 9×10^4 cd/m² @ 80 A/cm² and 143° respectively. The specific luminance change of the pattern from 5 to 60 A/cm² is demonstrated in Fig. 7(h). At present, the realization of full-color micro-LED displays is predominantly grounded in quantum dot technology. Among the various methods, blue light excitation stands as the most commonly adopted approach. This preference arises from the fact that, when compared to UV light, blue light necessitates only two distinct quantum dot colors for achieving a full-color spectrum. Moreover, the utilization of blue light eliminates concerns about potential ultraviolet light leakage and its implications for human exposure. Consequently, GaN-on-GaN blue light micro-LEDs, distinguished by their elevated luminance and uniformity, confer a unique set of advantages. These advantages are particularly pronounced in the context of achieving a wider color gamut, facilitating high-energy excitation, and enabling displays with elevated resolution.

Conclusion

In this paper, we comprehensively compare GaN-on-GaN and GaN-on-Sapphire micro-LEDs from the epitaxial to display application perspectives. At the epitaxial level, we achieved an ultra-low dislocation density in GaN-on-GaN, which is three orders of magnitude lower than that in GaN-on-Sapphire. The TRPL results reveal that the

GaN-on-GaN structure manifests a reduced carrier lifetime and a notable diminished QCSE. Moving on to device characterization, we present two variations of blue-emitting devices on different substrates, along with green-emitting devices on GaN-on-GaN. The GaN-on-GaN devices exhibit excellent electrical and optical attributes, such as reduced ideality factors and series resistances, stable central wavelengths, narrower FWHM, and diminished EQE droop. Moreover, through fitting calculations of IQE and EL spectra of blue-emitting devices on different substrates, we ascertain the presence of more pronounced deep-level trap-assisted recombination within sapphire-substrate devices, closely tied to the epitaxial dislocation density. Lastly, in the realm of display applications, GaN-on-GaN micro-displays manifest improved display uniformity and higher brightness. This factor plays a pivotal role in paving the way for the imminent realization of high-brightness, fine-pitch, and high-resolution AR displays.

Materials and methods

The study involved the growth of GaN-based micro-LED epi-layer structures on both a 2-inch standard c-plane sapphire substrate and a free-standing GaN substrate (as shown in Fig. 1 (b1)) using metal organic chemical vapour deposition (MOCVD). The growth process for both substrates was conducted under identical conditions. The only difference is an unintentionally doped GaN buffer layer was grown on the sapphire substrate firstly. The epitaxial layers were sequentially deposited in the following order: a 1800-nm Si-doped n-GaN layer, a 20 nm Si-doped n-Al_{0.05}Ga_{0.95}N electron spreading layer (ESL), a stress-relaxation layer (SRL) comprising 3 periods of u-In_{0.05}GaN (1 nm)/n-GaN (49 nm), a 22 nm 2 periods of multiple quantum wells (MQWs) region consisting of u-In_xGaN (3 nm)/n-GaN (8 nm) with indium components x of 0.15, and 0.25 for blue and green emission respectively, a 20 nm Mg-doped low temperature (LT) p-GaN layer, a 20 nm p-Al_{0.05}GaN electron blocking layer, and a 40 nm Mg-doped high temperature (HT) p-GaN layer. The specific structure is demonstrated in Fig. S2(a) in Supplementary Information.

To enhance current spreading, an initial deposition of a 100-nm indium tin oxide (ITO) layer onto p-GaN was carried out using E-beam technology. Subsequently, the ITO layer was annealed at 550 °C with 100% O₂ for 5 min to increase transparency and at 600 °C with 80% N₂ and 20% O₂ for 3 min to enhance conductivity through rapid thermal annealing, thereby achieving an ohmic contact between ITO and p-GaN. Next, photolithography was employed with a 300 nm PECVD SiO₂ layer as a hard mask to define the mesa structure, as shown in Fig. S2(b). Inductively coupled plasma (ICP) etching using BCl₃/Cl₂ = 12/12 SCCM for ITO and BCl₃/Cl₂ = 5/25 SCCM for p-GaN was utilized to etch the ITO current spreading layer (CSL) and p-GaN, respectively. Following that, the device was immersed in an 8% KOH solution at 80 °C to reduce sidewall damage caused by the ICP process and eliminate nano-defects formed during the ITO dry etching. Subsequently, a dual-layer passivation with a 50-nm thermal ALD Al₂O₃ (trimethylaluminum (TMA) + H₂O) layer and a 400-nm PECVD SiO₂ layer were deposited to passivate the remaining sidewall dangling bonds. For the p-electrode and n-electrode, a 300 nm Ti/Al/Ni/Au stack layer was evaporated onto the ITO and n-GaN, respectively, using photolithography and E-beam techniques. This stack layer also served as the indium penetration blocking

layer, as shown in Fig. S2(c). Lastly, a 2- μm thick indium layer was deposited onto the passivation layer and connected with both p- and n-electrodes, which is ready for reflow and flip-chip bonding process. Upon completion of this step, the display chip on the LED epitaxial structure has been fabricated, as depicted in Fig. 1(b2).

The 2-inch wafer is subjected to a series of post-fabrication processes for micro-LED display, including grinding, rough polishing by using Galaxy GS610P Precision Polishing Machine and chemical mechanical polishing (CMP) by using AM Technology Single Side Polishing Machine ASP Series to thin the thickness down to 280 μm . Then, display chips are obtained by laser dicing from the 2-inch wafer by using Hanslaser DSI-9200 automatic invisible dicing machine, as shown in Fig. 1(b3). The chips undergo a subsequent treatment with 1% HCl to enhance the formation of indium spheres. Subsequently, reflow process is accomplished in an acidic gas environment (HCOOH), with an operating temperature of 200°C, and the process duration lasting 2 min in ATV SRO-700 reflow system. After the reflow process, the indium metal forms spheres, which help to enhance the connection of solder joints on the micro-LED display chip to the driver chip, thereby improving the reliability of the soldering. Fig. S2(d) and Fig. 7(c)-(f) respectively illustrate the schematic diagram and SEM images of the indium metal after reflowing into spheres. Following this, the mass transfer of the micro-LED display chip and driver chip can be achieved through chip-to-chip bonding. The micro-LED display chips are transferred to ACC μ RA100 flip-chip bonder with a $\pm 0.5 \mu\text{m}$ placement accuracy. The force and temperature are 43 kg and 200°C, and process duration is 240 s. The outcomes of chip-to-chip bonding are showcased in Fig. S13, wherein the FIB-SEM images of Fig. S13(a) and (b) vividly demonstrate the seamless integration of the display chip and driver chip through the utilization of indium bumps. Due to the active matrix driving method, each pixel of the display chip has its corresponding independent driving circuit, as the 2T1C structure in our case. The layout design of the 2T1C driver, including clock signal (CLK), scanning signal (V_{scan}), and partition signal (Data1, 2, 3, etc.), is illustrated in Fig. S13(c) and (d). The inset in Fig. S13(d) depicts the schematic diagram of the 2T1C circuit. The panel luminance and field of view (FOV) is measured by using SITAN-LDM3 Optical Spectrometer (the measurement setup can be referred to Fig. S14).

Supplementary Information

The online version contains supplementary material available at <https://doi.org/10.1186/s43074-024-00137-4>.

Supplementary Material 1.

Acknowledgements

The authors would like to thank Shenzhen Sitan Technology, Nanosystem Fabrication Facility (NFF) and E-pack Lab in HKUST for technical support to accomplish the fabrication and characterization in this work. The authors would also like to thank Dr. Zhibo Sun, and Prof. Jr-Hau He from CityU of Hong Kong for their valuable discussion.

Authors' contributions

Conceptualization: Zhaojun Liu, Hoi-Sing Kwok, Ke Xu. Methodology: Yibo Liu, Guobin Wang, Zhaojun Liu, Ke Xu. Investigation: Yibo Liu, Guobin Wang, Feng Feng, Mengyuan Zhanghu, Zichun Li. Visualization: Yibo Liu, Guobin Wang, Zhengnan Yuan, Zichun Li. Funding acquisition: Zhaojun Liu, Hoi-Sing Kwok. Project administration: Zhaojun Liu, Hoi-Sing Kwok. Supervision: Zhaojun Liu, Hoi-Sing Kwok, Ke Xu. Writing – original draft: Yibo Liu, Feng Feng, Zhengnan Yuan, Zichun Li. Writing – review & editing: Zhaojun Liu, Hoi-Sing Kwok.

Funding

This work was supported by the National Key R&D Program of China under Grant No. 2023YFB2806800; Fundamental and Applied Fundamental Research Fund of Guangdong Province (No.2021B1515130001); Shenzhen Science and Technology Program (No.JCYJ20220818100603007).

Availability of data and materials

Data underlying the results presented in this paper are not publicly available at this time but may be obtained from the authors upon reasonable request.

Declarations

Competing interests

The authors declare no conflicts of interest.

Received: 12 April 2024 Revised: 2 July 2024 Accepted: 15 July 2024

Published online: 14 August 2024

References

- Liu Z, Lin CH, Hyun BR, Sher CW, Lv Z, Luo B, et al. Micro-light-emitting diodes with quantum dots in display technology. *Light Sci Appl*. 2020;9(1):83.
- Peng D, Zhang K, Liu Z. Design and Fabrication of fine-pitch pixelated-addressed micro-LED Arrays on printed circuit board for display and communication applications. *IEEE J Electron Devices Soc*. 2017;5(1):90–4.
- Liu Z, Chong WC, Wong KM, Lau KM. GaN-based LED micro-displays for wearable applications. *Microelectron Eng*. 2015;148:98–103.
- Huang Y, Hsiang EL, Deng MY, Wu ST. Mini-LED, Micro-LED and OLED displays: present status and future perspectives. *Light Sci Appl*. 2020;9(1):105.
- Wu T, Sher CW, Lin Y, Lee CF, Liang S, Lu Y, et al. Mini-LED and micro-LED: promising candidates for the next generation display technology. *Appl Sci*. 2018;8(9):1557.
- Lan HY, Tseng IC, Lin YH, Lin GR, Huang DW, Wu CH. High-speed integrated micro-LED array for visible light communication. *Opt Lett*. 2020;45(8):2203.
- Xie E, He X, Islim MS, Purwita AA, McKendry JJD, Gu E, et al. High-speed visible light communication based on a III-nitride series-biased micro-LED array. *J Lightwave Technol*. 2019;37(4):1180–6.
- Liu X, Wang L, Zhang C, Liu C, Lv Z, Liu Z, et al. Micro-LED with red-green-blue super-pixel integration for simultaneous display and optical near field communication. *Opt Express*. 2022;30(14):24889.
- Lee JH, Ahn Y, Lee HE, Jang YN, Park AY, Kim S, et al. Wearable surface-lighting micro-light-emitting diode patch for melanogenesis inhibition. *Adv Healthcare Materials*. 2023;12(1):2201796.
- Lee HE, Shin JH, Park JH, Hong SK, Park SH, Lee SH, et al. Micro light-emitting diodes for display and flexible biomedical applications. *Adv Funct Materials*. 2019;29(24):1808075.
- Yin K, Hsiang EL, Zou J, Li Y, Yang Z, Yang Q, et al. Advanced liquid crystal devices for augmented reality and virtual reality displays: principles and applications. *Light Sci Appl*. 2022;11(1):161.
- Lee YH, Zhan T, Wu ST. Prospects and challenges in augmented reality displays. *Virtual Real Intell Hardware*. 2019;1(1):10–20.
- Dai Q, Shan Q, Cho J, Schubert EF, Crawford MH, Koleske DD, et al. On the symmetry of efficiency-versus-carrier-concentration curves in GaInN/GaN light-emitting diodes and relation to droop-causing mechanisms. *Appl Phys Lett*. 2011;98(3):033506.
- Piprek J. Efficiency droop in nitride-based light-emitting diodes. *Physica Status Solidi (a)*. 2010;207(10):2217–25.
- Vampola KJ, Iza M, Keller S, DenBaars SP, Nakamura S. Measurement of electron overflow in 450 nm InGaN light-emitting diode structures. *Appl Phys Lett*. 2009;94(6):061116.
- Akita K, Nakamura T, Hirayama H. Advantages of GaN substrates in InAlGaN quaternary ultraviolet-light-emitting diodes. *Jpn J Appl Phys*. 2004;43(12):8030–1.
- Li G, Wang W, Yang W, Lin Y, Wang H, Lin Z, et al. GaN-based light-emitting diodes on various substrates: a critical review. *Rep Prog Phys*. 2016;79(5):056501.
- Miskys CR, Kelly MK, Ambacher O, Stutzmann M. Freestanding GaN-substrates and devices. *Phys Stat Sol (c)*. 2003;6:1627–50.
- Li Z, Liu Y, Feng F, Zhanghu M, Kwok HS, Liu Z. –3: Exploring the temperature dependence of GaN-on-GaN homoepitaxy micro-LEDs. *Symp Digest of Tech Papers*. 2023;54(1):406–9.
- Mukai T, Takekawa K, Nakamura S. InGaN-based blue light-emitting diodes grown on epitaxially laterally overgrown GaN substrates. *Jpn J Appl Phys*. 1998;37(7B):L839.
- Akita K, Kyono T, Yoshizumi Y, Kitabayashi H, Katayama K. Improvements of external quantum efficiency of InGaN-based blue light-emitting diodes at high current density using GaN substrates. *J Appl Phys*. 2007;101(3):033104.
- Liu Z, Wei T, Guo E, Yi X, Wang L, Wang J, et al. Efficiency droop in InGaN/GaN multiple-quantum-well blue light-emitting diodes grown on free-standing GaN substrate. *Appl Phys Lett*. 2011;99(9):091104.
- Chao C-L, Xuan R, Yen H-H, Chiu C-H, Fang Y-H, Li Z-Y, et al. Reduction of efficiency droop in InGaN Light-emitting diode grown on self-separated freestanding GaN substrates. *IEEE Photon Technol Lett*. 2011;23(12):798–800.
- Kim DH, Park YS, Kang D, Kim KK, Seong TY, Amano H. Combined effects of V pits and chip size on the electrical and optical properties of green InGaN-based light-emitting diodes. *J Alloy Compd*. 2019;796:146–52.

25. Liou JK, Liu YJ, Chen CC, Chou PC, Hsu WC, Liu WC. On a GaN-based light-emitting diode with an aluminum metal mirror deposited on naturally-textured V-shaped pits grown on the p-GaN surface. *IEEE Electron Device Lett.* 2012;33(2):227–9.
26. Koike K, Lee S, Cho SR, Park J, Lee H, Ha JS, et al. Improvement of Light extraction efficiency and reduction of leakage current in GaN-based LED via V-Pit formation. *IEEE Photon Technol Lett.* 2012;24(6):449–51.
27. Zhou S, Liu S, Ding H. Enhancement in light extraction of LEDs with SiO₂ current blocking layer deposited on naturally textured p-GaN surface. *Opt Laser Technol.* 2013;47:127–30.
28. Okada N, Kashiwara H, Sugimoto K, Yamada Y, Tadatomo K. Controlling potential barrier height by changing V-shaped pit size and the effect on optical and electrical properties for InGaN/GaN based light-emitting diodes. *J Appl Phys.* 2015;117(2):025708.
29. Wu X, Liu J, Jiang F. Hole injection from the sidewall of V-shaped pits into c-plane multiple quantum wells in InGaN light emitting diodes. *J Appl Phys.* 2015;118(16):164504.
30. Kim J, Cho YH, Ko DS, Li XS, Won JY, Lee E, et al. Influence of V-pits on the efficiency droop in InGaN/GaN quantum wells. *Opt Express.* 2014;22(S3):A857.
31. Tomiya S, Kanitani Y, Tanaka S, Ohkubo T, Hono K. Atomic scale characterization of GaInN/GaN multiple quantum wells in V-shaped pits. *Appl Phys Lett.* 2011;98(18):181904.
32. Kim J, Kim J, Tak Y, Chae S, Kim JY, Park Y. Effect of V-shaped Pit size on the reverse leakage current of InGaN/GaN light-emitting diodes. *IEEE Electron Device Lett.* 2013;34(11):1409–11.
33. Chang CY, Li H, Shih YT, Lu TC. Manipulation of nanoscale V-pits to optimize internal quantum efficiency of InGaN multiple quantum wells. *Appl Phys Lett.* 2015;106(9):091104.
34. Zhou S, Liu X, Yan H, Gao Y, Xu H, Zhao J, et al. The effect of nanometre-scale V-pits on electronic and optical properties and efficiency droop of GaN-based green light-emitting diodes. *Sci Rep.* 2018;8(1):11053.
35. Samsudin MEA, Alias EA, Md Taib MI, Li H, Iza M, Denbaars SP, et al. Limiting factors of GaN-on-GaN LED. *Semicond Sci Technol.* 2021;36(9):095035.
36. Romanitan C, Mihalache I, Tutunaru O, Pachiu C. Effect of the lattice mismatch on threading dislocations in heteroepitaxial GaN layers revealed by X-ray diffraction. *J Alloy Compd.* 2021;858:157723.
37. Davydov VYu, Kitaev YuE, Goncharuk IN, Smirnov AN, Graul J, Semchinova O, et al. Phonon dispersion and Raman scattering in hexagonal GaN and AlN. *Phys Rev B.* 1998;58(19):12899–907.
38. James Singh K, Huang YM, Ahmed T, Liu AC, Huang Chen SW, Liou FJ, et al. Micro-LED as a promising candidate for high-speed visible light communication. *Appl Sci.* 2020;10(20):7384.
39. Liu Y, Zhang K, Feng F, Chan K, Yeung S, Kwok H, et al. The size and temperature effect of ideality factor in GaN/InGaN multiple quantum wells micro-light-emitting diodes. *J Soc Info Display.* 2021;29(12):948–60.
40. Zhu D, Xu J, Noemaun AN, Kim JK, Schubert EF, Crawford MH, et al. The origin of the high diode-ideality factors in GaInN/GaN multiple quantum well light-emitting diodes. *Appl Phys Lett.* 2009;94(8):081113.
41. Liu Y, Zhanghu M, Feng F, Li Z, Zhang K, Kwok HS, et al. Identifying the role of carrier overflow and injection current efficiency in a GaN-based micro-LED efficiency droop model. *Opt Express.* 2023;31(11):17557.
42. Han DP, Kim H, Shim JI, Shin DS, Kim KS. Influence of carrier overflow on the forward-voltage characteristics of InGaN-based light-emitting diodes. *Appl Phys Lett.* 2014;105(19):191114.
43. Sang L, Ren B, Endo R, Masuda T, Yasufuku H, Liao M, et al. Boosting the doping efficiency of Mg in p-GaN grown on the free-standing GaN substrates. *Appl Phys Lett.* 2019;115(17):172103.
44. Wang L, Jin J, Mi C, Hao Z, Luo Y, Sun C, et al. A Review on experimental measurements for understanding efficiency droop in InGaN-based light-emitting diodes. *Materials.* 2017;10(11):1233.
45. Shim JI, Shin DS. Measuring the internal quantum efficiency of light-emitting diodes: towards accurate and reliable room-temperature characterization. *Nanophotonics.* 2018;7(10):1601–15.
46. Olivier F, Daami A, Licitra C, Templier F. Shockley-Read-Hall and Auger non-radiative recombination in GaN based LEDs: a size effect study. *Appl Phys Lett.* 2017;111(2):022104.
47. Jeong H, Salas-Montiel R, Lerondel G, Jeong MS. Indium gallium nitride-based ultraviolet, blue, and green light-emitting diodes functionalized with shallow periodic hole patterns. *Sci Rep.* 2017;7(1):45726.
48. Takeuchi T, Sota S, Katsuragawa M, Komori M, Takeuchi H, Hiroshi Amano HA, et al. Quantum-confined stark effect due to piezoelectric fields in GaInN strained quantum wells. *Jpn J Appl Phys.* 1997;36(4A):L382.
49. Tsai SC, Lu CH, Liu CP. Piezoelectric effect on compensation of the quantum-confined Stark effect in InGaN/GaN multiple quantum wells based green light-emitting diodes. *Nano Energy.* 2016;28:373–9.
50. Li JZ, Tao YB, Chen ZZ, Jiang XZ, Fu XX, Jiang S, et al. Quasi-homoepitaxial GaN-based blue light emitting diode on thick GaN template. *Chinese Phys B.* 2014;23(1):016101.
51. Horng RH, Ye CX, Chen PW, Iida D, Ohkawa K, Wu YR, et al. Study on the effect of size on InGaN red micro-LEDs. *Sci Rep.* 2022;12(1):1324.
52. Liu Y, Zhang K, Hyun BR, Kwok HS, Liu Z. High-brightness InGaN/GaN micro-LEDs with secondary peak effect for displays. *IEEE Electron Device Lett.* 2020;41(9):1380–3.
53. Wang L, Lu C, Lu J, Liu L, Liu N, Chen Y, et al. Influence of carrier screening and band filling effects on efficiency droop of InGaN light emitting diodes. *Opt Express.* 2011;19(15):14182.
54. Robertson AR. The CIE color-difference formulae. *Color Res Appl.* 1977;2(1):7–11.
55. Melgosa M, Hita E, Romero J, del Barco LJ. Color-discrimination thresholds translated from the CIE (x, y, z) space to the CIE 1976 (L*, a*, b*). *Color Res Appl.* 1994;19(1):10–8.
56. Perduijn A, De Krijger S, Claessens J, Kaito N, Yagi T, Hsu ST, et al. 43.2: Light output feedback solution for RGB LED backlight applications. *Symp Digest of Tech Papers.* 2003;34(1):1254–7.
57. Lu B, Wang Y, Hyun BR, Kuo HC, Liu Z. Color difference and thermal stability of flexible transparent InGaN/GaN Multiple quantum wells mini-LED arrays. *IEEE Electron Device Lett.* 2020;41(7):1040–3.
58. Xu F, Wang G, Tao T, Zhuang Z, Yan QA, Zhi T, et al. Optimized InGaN/GaN Quantum structure for high-efficiency micro-LEDs displays with low current injection. *IEEE Trans Electron Devices.* 2023;70(8):4257–63.
59. Chen CJ, Chen HC, Liao JH, Yu CJ, Wu MC. Fabrication and characterization of active-matrix 960×540 blue GaN-based micro-LED display. *IEEE J Quantum Electron.* 2019;55(2):1–6.

60. Smith JM, Ley R, Wong MS, Baek YH, Kang JH, Kim CH, et al. Comparison of size-dependent characteristics of blue and green InGaN microLEDs down to 1 μm in diameter. *Appl Phys Lett*. 2020;116(7):071102.
61. Liu Y, Feng F, Zhang K, Jiang F, Chan KW, Kwok HS, et al. Analysis of size dependence and the behavior under ultrahigh current density injection condition of GaN-based Micro-LEDs with pixel size down to 3 μm . *J Phys D: Appl Phys*. 2022;55(31):315107.
62. Kirilenko P, Iida D, Zhuang Z, Ohkawa K. InGaN-based green micro-LED efficiency enhancement by hydrogen passivation of the p-GaN sidewall. *Appl Phys Express*. 2022;15(8):084003.
63. Zhu S, Shan X, Lin R, Qiu P, Wang Z, Lu X, et al. Characteristics of GaN-on-Si green micro-LED for Wide color gamut display and high-speed visible light communication. *ACS Photonics*. 2023;10(1):92–100.
64. Shin Y, Park J, Bak BU, Min S, Shin DS, Park JB, et al. Investigation and direct observation of sidewall leakage current of InGaN-Based green micro-light-emitting diodes. *Opt Express*. 2022;30(12):21065.

Publisher's Note

Springer Nature remains neutral with regard to jurisdictional claims in published maps and institutional affiliations.